DNA Hairpin, Pseudoknot, and Cruciform Stability in a Solvent-Free Environment

Erin Shammel Baker, Nicholas F. Dupuis, and Michael T. Bowers*

Department of Chemistry and Biochemistry, University of California, Santa Barbara, California 93106-9510

Received: August 22, 2008; Revised Manuscript Received: October 30, 2008

The secondary structures of DNA hairpins, pseudoknots and cruciforms are of great interest because of their possible role in materials applications and biological functions such as regulating transcription. To determine the stability of these structures, DNA sequences capable of forming each were analyzed with mass spectrometry, ion mobility, and molecular dynamics calculations. Nano-ESI mass spectra indicated that stoichiometries compatible with hairpin, pseudoknot, and cruciform structures were present. Ion mobility spectrometry (IMS) was utilized to obtain experimental collision cross sections for all complexes. These cross sections were compared with structures from molecular dynamics, and in all cases, the lowest-charge states could be matched with a structure for an intact hairpin, pseudoknot, or cruciform. However, as the charge states of the single-stranded hairpins and pseudoknots increased, their structures elongated, and all Watson−Crick pairs were broken.

Introduction

In 1953, Watson and Crick characterized the first secondary structure of DNA as a double-stranded, antiparallel, right-handed helix.[1] However, although the Watson−Crick (WC) helix conformation is the most abundant form of DNA, it is not the only form. In fact, in the past 50 years, many single- and multiple-stranded DNA complexes that are not WC helices have been observed. Three DNA secondary structures of great interest are single-stranded hairpins and pseudoknots[2] and double-stranded cruciforms,[3] which all have intermolecular loops and WC paired stem regions. Although these conformations are only a small percentage of DNA secondary structures, they have been the focus of a large amount of research because of their possible role in regulating transcription[4−6] and in proposed biosensor and materials applications.[7−10]

To study the single-stranded hairpin and pseudoknot conformations of DNA, two sequences were designed. The first sequence was created to produce only a hairpin structure, whereas the second was designed to form a hairpin, a pseudoknot, or both (Scheme 1). For simplicity, the self-complementary inverted hairpin sequence [dTGCGATACTCATCGCA] and hairpin/pseudoknot sequence [dGCGAT$_3$CTGAC$_2$GCT$_6$GT CAG] are referred to herein as HP and PK, respectively. Because PK has the possibility of forming both hairpin and pseudoknot structures, the energies of the two forms can be compared to understand which structure is more energetically favorable or whether they coexist. A cruciform was also designed from the complementary sequences CF1 [d(C$_2$G$_2$)$_2$ATA(CG)$_4$] and CF2 [d(CG)$_4$ATA(C$_2$G$_2$)$_2$]. These cruciform sequences were chosen because they do not have complementary ends (CCGG versus CGCG), so hairpin formation is not possible for the single strands and cannot compete with the abundance of double-stranded cruciform structures. To probe the structure of these various sequences, nanoelectrospray mass spectrometry (nano-ESI-MS) combined with ion mobility spectrometry (IMS) was utilized.[11−13] Comparisons of solution-phase and solvent-free structures were made, along with the effect of charge state on the stability of each structure.

* E-mail: bowers@chem.ucsb.edu.

Experimental Methods

Materials and Sample Preparation. HP, PK, CF1, and CF2 (Scheme 1) were purchased from Integrated DNA Technologies, Inc. (Coralville, IA) and used without further purification. To prepare solutions for analysis, HP, PK, CF1, and CF2 were suspended to a concentration of 300 μM in a 30 mM NH$_4$OAc/H$_2$O buffer solution (pH 7). CF1 and CF2 were then mixed together in a 1:1 ratio. The HP, PK, and CF1/CF2 mixtures were annealed at 95 °C for 10 min, slowly cooled to room temperature over a time period of 8 h, and stored at 10 °C. All of the solutions were diluted to 50 μM with H$_2$O before being analyzed. A high-ionic-strength buffer solution (final concentration of 5 mM NH$_4$OAc/H$_2$O) was utilized to stabilize the structures present in the HP, PK, and CF1/CF2 mixtures and to help provide an intense nano-ESI signal.

Mass Spectrometry and Ion Mobility Experiments. The experiments in this work were performed on a home-built ESI-IMS-MS instrument that was previously described in detail,[14] so only a brief description is given here. Ions were generated by nano-ESI and injected into an ion funnel through a 3-in.-long capillary. The ion funnel essentially acted as an ion guide, compressing and dehydrating the stream of ions exiting the capillary and directing them toward the drift cell. For mass spectrometry analysis, the ions continuously flowed through the funnel into the drift cell, a specific mass range was scanned by a quadrupole mass filter, and then the ions were detected. For the IMS studies, the funnel was used as an ion trap, allowing conversion of the continuous ion beam from the ESI source into a pulsed signal by storing the ions for 1 ms and then releasing them in a short 10-μs ion pulse. The injection voltage was kept to a minimum (20 V) in all studies to avoid structural changes of the ions. After the ions entered the 4.5-cm-long drift cell in the IMS analyses, they were quickly thermalized by collisions with ~5 Torr of helium gas and drifted through the cell under the influence of a weak, uniform electric field (10−23 V/cm). Collisions with the helium buffer gas broadened the ion packet and served to bring a balance between the force imposed by the electric field and the frictional drag force. As a consequence, the ions drifted at a constant velocity, v_d, proportional to the applied field E

10.1021/jp807529m CCC: $40.75
Published on Web 01/20/2009

$$v_d = KE \quad (1)$$

The proportionality constant, K, is termed the mobility of the ions, and when K is converted to a reduced mobility (K_o) at standard temperature and pressure, eq 1 becomes

$$t_A = \frac{l^2}{K_o}\frac{273.16}{760T}\frac{p}{V} + t_o \quad (2)$$

where l is the length of the drift cell, V is the voltage across the cell, p is the cell pressure, T is the cell temperature, and t_o is the time the ions spend between exiting the cell and reaching the detector. Hence, a plot of t_A versus p/V gives a straight line with an intercept of t_o and a slope proportional to $1/K_o$. The cross section can be readily determined from K_o using kinetic theory.[15]

Theoretical Calculations for Model Structures. Structural information about the ion mobility experiments was obtained by comparing the experimental cross sections determined from the arrival time distributions (ATDs) to cross sections of theoretical structures. HyperChem[16] was utilized to create the hairpin and pseudoknot starting structures for the DNA sequences HP and PK, whereas canonical A- and B-form helix starting geometries for the double-stranded CF1/CF2 structure were fashioned using the NUCGEN utility within AMBER 7.[17] Molecular dynamics simulations at 300 K were run on each structure for 2 ns using AMBER 7, and after every 5 ps, a structure was saved. Each structure was then energy-minimized, and its cross section was calculated using hard-sphere scattering and trajectory models developed by the Jarrold group.[18,19] In the calculations, the starting structures eventually converged to give at least one steady-state structure in which the cross section remains relatively constant. The average cross section of the final 50−100 structures in each steady state was used for comparison with the experimental values.

A series of simulated annealing/energy-minimization cycles was also used to obtain low-energy globular structures of each complex.[20−22] In this cycle, the initial structures were energy-minimized, annealed at 700 K for 30 ps (to allow the structure to overcome low-lying barriers and change shape), exponentially cooled to 50 K over a variable time step, and energy-minimized again. The final structure was saved and used as the starting structure for another annealing/minimization cycle. This process was continued until 300 low-energy structures had been generated, and the average cross section of the lowest 5−10 kcal/mol structures was compared to the experimental values.

Results and Discussion

Mass Spectra. The nano-ESI mass spectra for HP, PK, and CF1/CF2 are shown in Figure 1. Single strands with multiple charge states were observed for HP (Figure 1a) and PK (Figure 1b), but no double-stranded peaks were present for either sequence. The lack of double-stranded complexes in the mass spectra indicates that HP and PK do not form any type of self-complementary cruciform structure, even though they were slowly cooled after annealing for 8 h. Whereas two PK strands would have too many mismatched bases to form a double-stranded cruciform, two HP strands would have only three mismatches, making it possible for a double-stranded complex to exist. Other short self-complementary DNA strands (<23 bases) with three mismatches in their center were also examined to understand why HP did not form a double-stranded cruciform.

SCHEME 1: Schematic of the Three Sequences Analyzed: (a) HP Can Form a Single-Stranded Hairpin; (b) PK Can Form a Single-Stranded Hairpin, Pseudoknot, or Both; and (c) (CF1·CF2) Is Designed to Form Only a Double-Stranded Cruciform Structure to Avoid Hairpin Interference

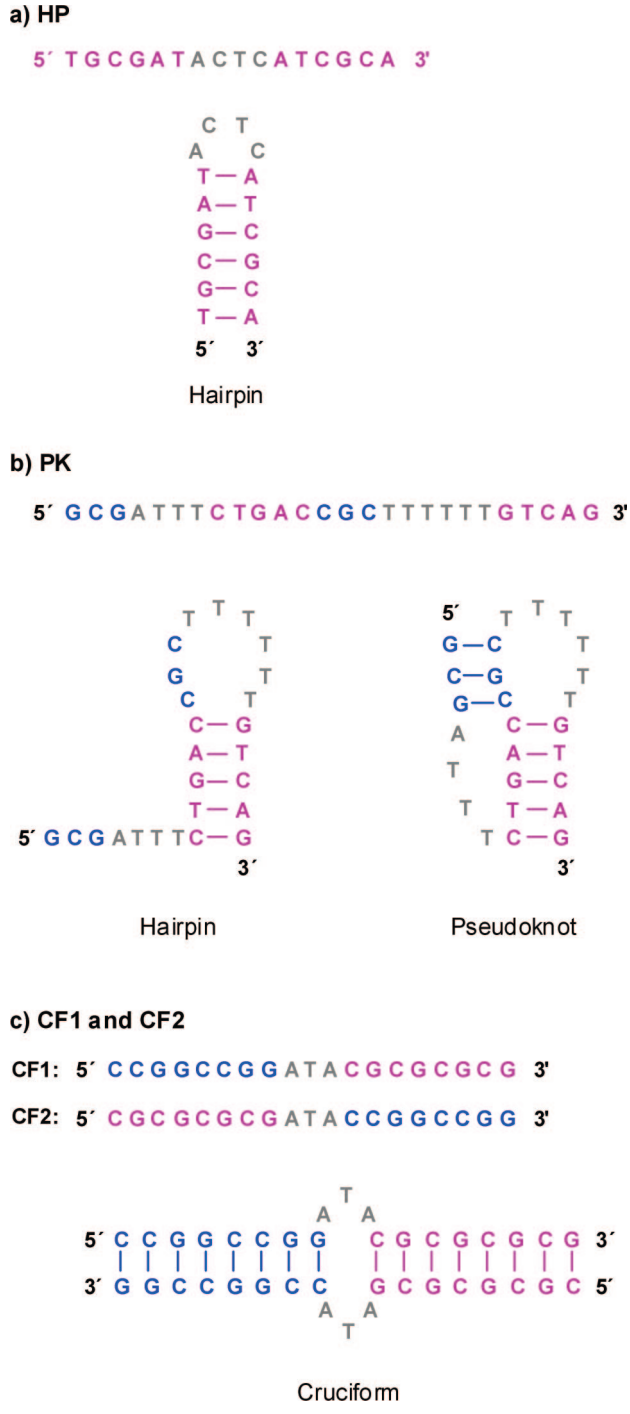

All of these short strands were slowly cooled after annealing, but none formed double-stranded complexes (consistent with the HP results in Figure 1a). Thus, single-stranded conformations appear to be energetically favored over mismatched double-stranded structures for short self-complementary DNA strands.

In contrast to HP and PK, the mass spectrum for the CF1/CF2 mixture showed peaks due to single strands of both CF1 and CF2 (CF1 and CF2 have the same mass) with multiple charge states, along with a double-stranded $(CF1\cdot CF2)^{11-}$

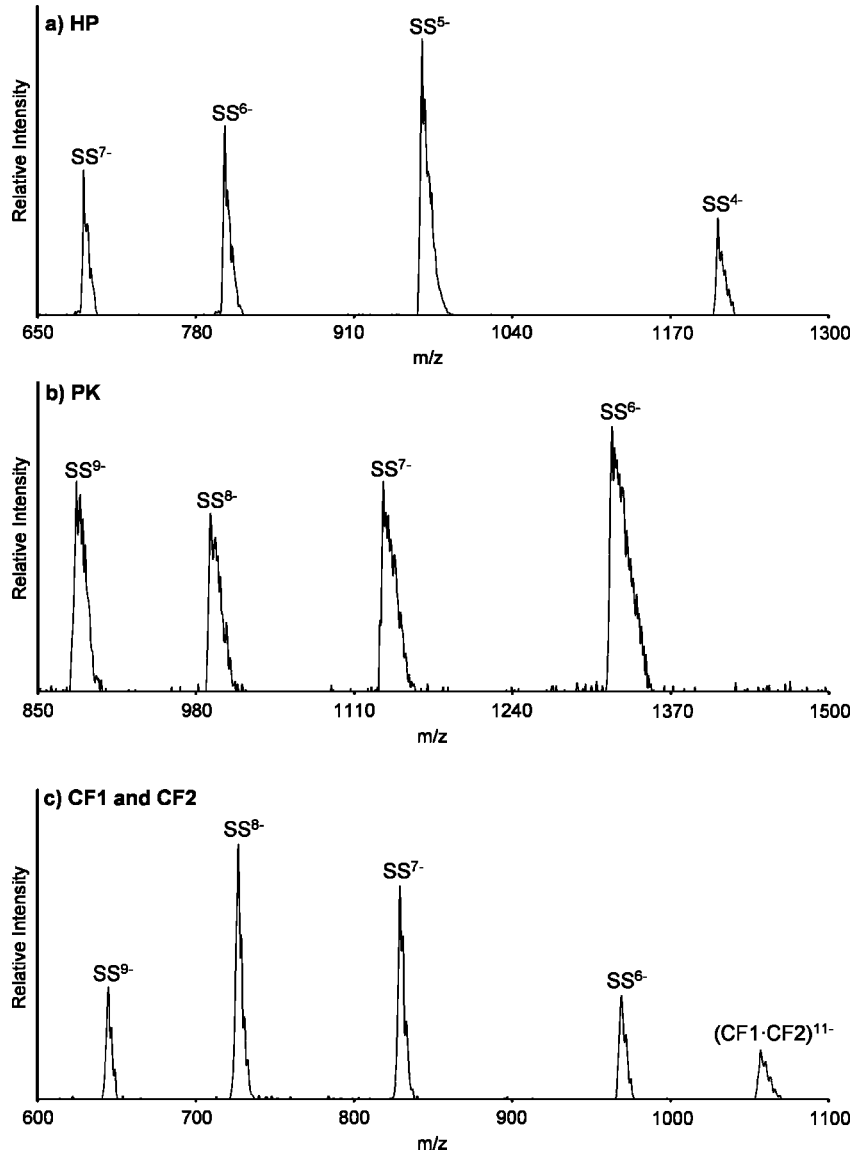

Figure 1. Nano-ESI mass spectra for (a) HP, (b) PK, and (c) CF1 combined with CF2. Only single strands (SSs) were observed for HP and PK, but a duplex was observed when CF1 and CF2 were combined. The peaks were broadened on the high-mass side by NH_4^+ adducts.

complex. This is an interesting result given the fact that there are three mismatched bases in the CF1/CF2 strands. However, neither strand can form a hairpin like HP because the ends are not complementary (CCGG versus CGCG), so it appears that cruciform formation is possible. Because the spectra in Figure 1 indicate that stoichiometries indicative of hairpins, pseudoknots, and cruciforms are present for HP, PK, and CF1/CF2, ion mobility analysis of each peak was necessary to determine whether these structures were actually present.

Ion Mobility. The IMS arrival time distributions (ATDs) for HP^{4-}, PK^{6-}, and $(CF1 \cdot CF2)^{11-}$ are presented in Figure 2. Single-peak ATDs were observed for all of the charge states of HP and PK, and these single symmetric peaks indicate that, most likely, only one family of conformers is present for each. The cross sections for each charge state were measured, and the values are reported in Table 1.

An interesting trend in the experimental cross sections of HP and PK can be observed (Table 1). As the charge states increase (become more negative) for both HP and PK, the cross sections also increase. Hoaglund et al. observed a similar trend when they studied single-stranded dT_{10} ions,[23] and their instrument did not utilize an ion funnel, indicating that it did not contribute to the observed increase in cross section. Molecular dynamics calculations at 300 K were performed to understand this observation.[17,24] The structure for HP and PK with the least negative charge state was analyzed first, given that, in both cases, it had the smallest cross section (most compact structure). A hairpin conformation was used as the starting structure for HP^{4-}, whereas PK^{6-} was placed in both a hairpin and pseudoknot

TABLE 1: Experimental and Theoretical Cross Sections (Å^2) for HP and PK

		theory[b]			
complex	expt[a]	globular	hairpin	pseudoknot	broken WC
HP^{4-}	622	575	620	–	–
HP^{5-}	718	578	–	–	722
HP^{6-}	811	574	–	–	814
HP^{7-}	909	582	–	–	913
PK^{6-}	902	862	975	910	–
PK^{7-}	1009	864	–	–	1010
PK^{8-}	1122	870	–	–	1126
PK^{9-}	1219	867	–	–	1225

[a] 1% reproducibility error. [b] ≤2% standard deviation.

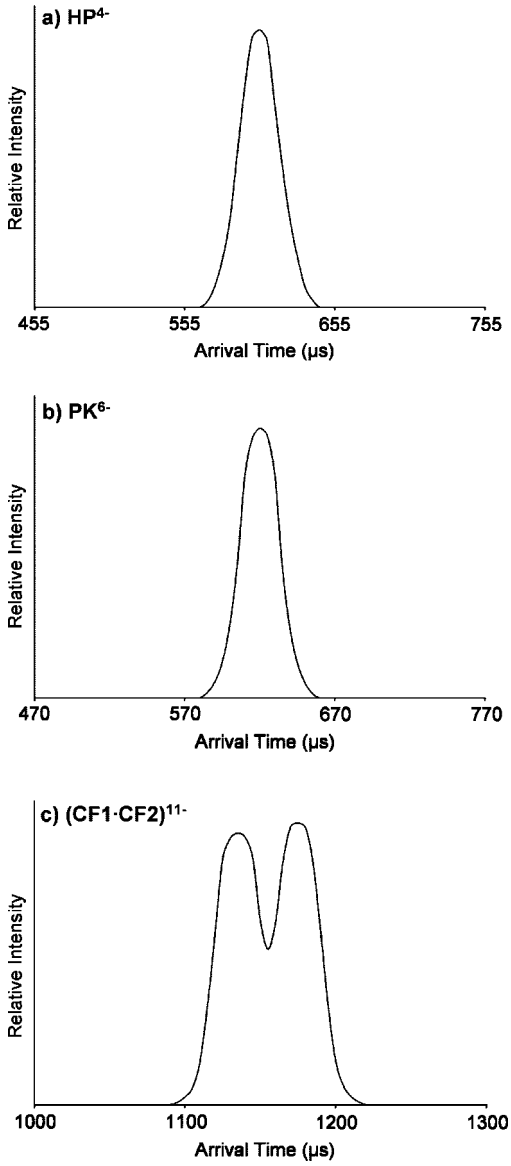

Figure 2. ATDs for (a) HP^{4-}, (b) PK^{6-}, and (c) $(CF1 \cdot CF2)^{11-}$. One peak is observed for all of the charges states of HP and PK, but two peaks are observed in the $(CF1 \cdot CF2)^{11-}$ ATD.

conformation (Scheme 1). Dynamics runs at 300 K were performed for each starting structure for 2 ns, and after every 5 ps, a structure was saved, and its cross section calculated. Only one steady state was observed in the dynamics plots (Figure 3) for all of the different starting structures, and the average cross section of the final 100 structures is listed in Table 1. Simulated annealing at 700 K was also used to generate globular structures for HP^{4-} and PK^{6-}, and the cross sections for the lowest-energy globular structures are also included in Table 1.

Representative structures of the HP^{4-} hairpin resulting from the 300 K molecular dynamics calculations and the HP^{4-} globular structure from simulated annealing are shown in Figure 4. All of the WC pairs are retained for the hairpin structure, whereas no WC pairs exist in the globular structure. When the theoretical cross sections for HP^{4-} were compared with the experimental cross sections, the hairpin conformer agreed within 2% error, but the globular structure was too small to match the experimental value with reasonable error. These results indicate that the hairpin conformer with the 4− charge state is formed in solution, retains its structure in the solvent-free experimental

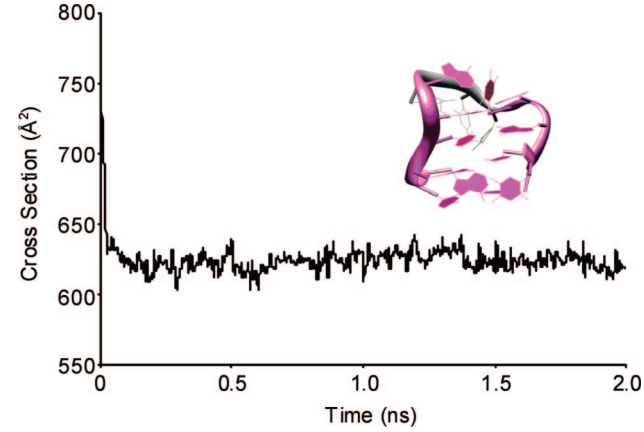

Figure 3. Plot of cross section versus dynamics time for HP^{4-}. The dynamics simulations were run at 300 K for 2 ns, and after every 5 ps, the structure was saved and its cross section calculated. Only one steady state was observed in the dynamics plots for each starting structure of HP and PK.

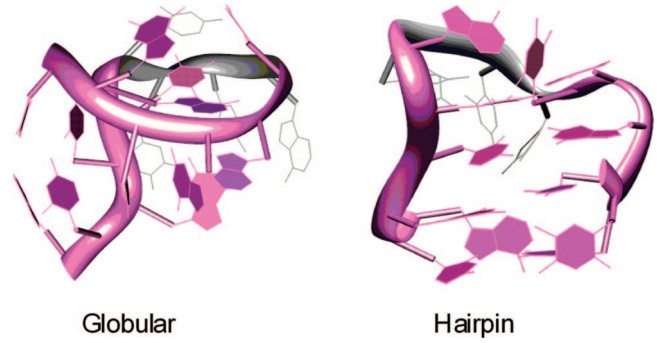

Figure 4. Theoretical structures for HP^{4-}. The globular structure is too small to match the experimental cross section, but the hairpin remaining after 2 ns of 300 K dynamics simulations correlates with the experimental cross section. The WC portion of HP is illustrated in pink.

environment, and does not convert to a globular structure within the experimental time scale (∼1 ms).

Theoretical structures for the PK^{6-} hairpin, pseudoknot, and globular complexes are shown in Figure 5. As in the hairpin structure of HP^{4-}, all of the WC pairs are retained in the hairpin and pseudoknot structures of PK^{6-}, whereas the globular structure has no WC pairing. When the cross sections for the hairpin, pseudoknot, and globular conformers of PK^{6-} were compared with the experimental cross section, only the pseudoknot agreed within 2%. The AMBER theoretical energies of the hairpin and pseudoknot structures with a 6− charge state were also compared to understand the stability of each structure. The pseudoknot was found to be 30 kcal/mol lower in energy than the hairpin conformation, probably because of the extra WC pairing interactions. However, the globular structure had the lowest energy of all of the structures (10 kcal/mol lower than the pseudoknot), but similar to HP^{4-}, the pseudoknot conformer is formed in solution for PK^{6-}, retains its structure in the solvent-free environment of the experiment, and does not convert to a globular structure within the experimental time scale.

To understand why the cross sections of HP and PK increase as their charge states becomes more negative, molecular dynamics simulations of the HP with charge states from −5 to −7 and of PK with charge states from −7 to −9 were analyzed. The same starting structures were utilized as for the lowest-energy charge states (HP^{4-} and PK^{6-}). For both HP and PK,

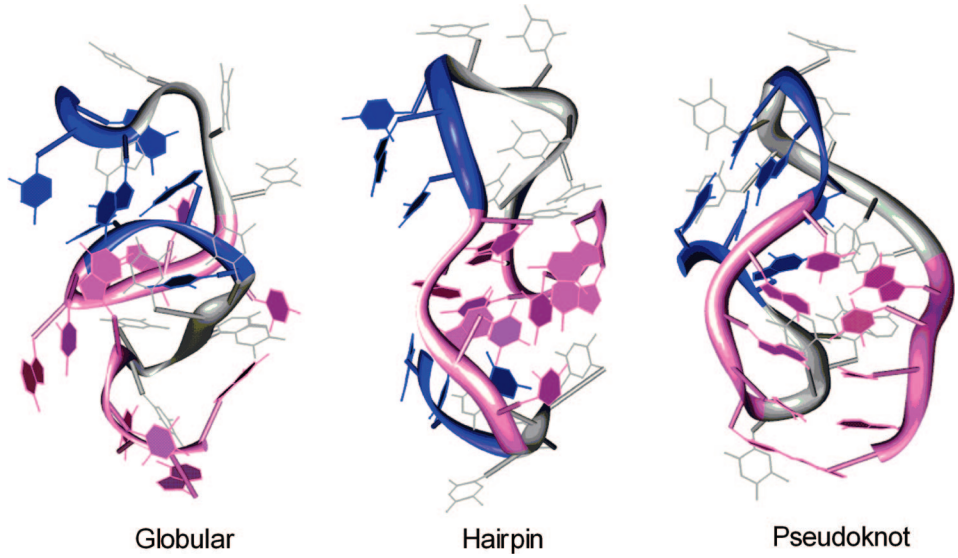

Figure 5. Theoretical structures for PK^{6-}. Only the pseudoknot correlates with the experimental cross section, as the globular structure is too small and the hairpin is too large. Coloring is based on Scheme 1, where the region with five consecutive WC pairs is shown in pink and the region with three WC pairs is blue.

TABLE 2: Experimental and Theoretical Cross Sections (Å^2) for (CF1·CF2)$^{11-}$

		theory[b]		
complex	expt[a]	A helix	B helix	globular
$(CF1 \cdot CF2)^{11-}$	1485 1653	1473	1638	1204

[a] 1% reproducibility error. [b] ≤2% standard deviation.

the globular structures were too small to match any of the experimental cross sections. However, as the charge states increased, the strands began to elongate, and the WC pairs broke in the hairpin structure of HP and in both the hairpin and pseudoknot conformations of PK, presumably as a result of charge repulsion (cross sections listed in Table 1 under "broken WC"). At the highest charge states observed experimentally for HP and PK, the structures were almost completely extended, as shown in Figure 6, and the cross sections of the elongated broken WC theoretical structures matched the experimental trend. For PK, both the hairpin and pseudoknot structures elongated into similar structures at the higher charge states. These results suggest that, as the higher charge states dehydrate in the ion funnel, Coulomb repulsion overcomes the stabilizing influence of the WC base pairing and the structures elongate, although elongated structures in solution at these charge states cannot be ruled out.

When the ATD for $(CF1 \cdot CF2)^{11-}$ was analyzed, two peaks were observed. These two peaks had cross sections of 1485 and 1653 Å^2 and signified the presence of two different conformers (Figure 2c). To determine the structure of each conformer in the experiment, theoretical modeling was utilized. Previous IMS measurements coupled with molecular dynamics simulations on duplexes from 8 to 30 bp indicated that both A- and B-form helices are observed for duplexes between 18 and 22 bp.[24−26] Because $(CF1 \cdot CF2)^{11-}$ has 19 bp, both A- and B-form helices were used as starting structures for 300 K molecular dynamics simulations. Only one steady state was observed for both the A- and B-form helices, and the three-base mismatch was popped open in the center of the cruciform, whereas all other WC pairs were retained. The A-form helix bent slightly and had a cross section of 1473 Å^2, whereas the B-form helix was more extended, with a cross section of 1638

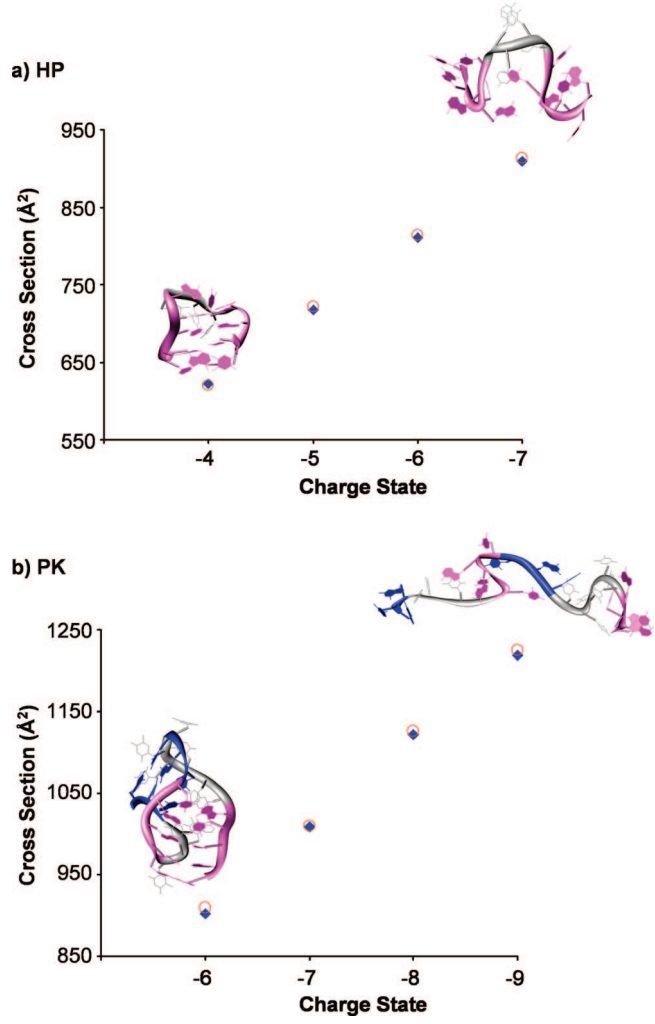

Figure 6. Charge state versus cross section plots for (a) HP and (b) PK. Experimental cross sections are shown with blue diamonds, and the closest matching theoretical cross sections are shown with red circles. As the charge states of HP and PK become more negative, the cross sections increase as a result of charge repulsion. The theoretical structures that correlate with these charges states form compact complexes at the least negative charge states, but are almost linear at the highest charge states.

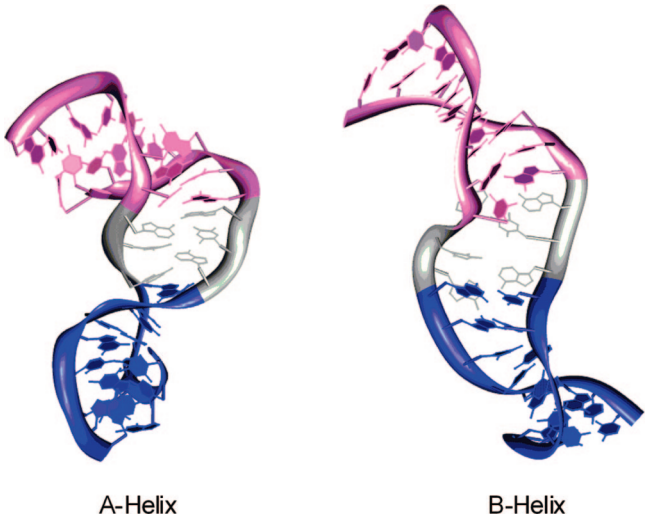

Figure 7. Theoretical structures for the A- and B-form helices of $(CF1 \cdot CF2)^{11-}$. The C_2G_2 repeat region is shown in blue, the CG repeat region is shown in pink, and the mismatch is gray, as indicated in Scheme 1.

Å^2 (Table 2 and Figure 7). Comparison of these theoretical cross sections with the experimental values showed that the A-form helix correlated with the shortest-time ATD peak, whereas the B-form helix agreed with the longest-time peak. The globular structure generated from simulated annealing did not match either peak, indicating that $(CF1 \cdot CF2)^{11-}$ coexisted as both A- and B-form cruciform helices under our solvent-free experimental conditions. Circular dichroism (CD) experiments were utilized to determine the solution-phase helix conformation of (CF1•CF2). CD is able to characterized whether DNA has an A-, B-, or Z-form helix in solution, as A-DNA has a maximum near 265 nm, B-DNA has a maximum near 280 nm, and Z-DNA has a maximum near 260 nm.[27−31] (CF1•CF2) had a spectrum indicative of only B-DNA, indicating that the solvent-free environment of mass spectrometry induced a partial B-to-A transition[32] for $(CF1 \cdot CF2)^{11-}$, causing both B- and A-form helices to be observed in the IMS experiments.[24−26]

Summary

The mass spectrometry, ion mobility, and molecular dynamics results presented for HP, PK, and (CF1•CF2) provide several important insights into the conformations of single-stranded and cruciform DNA. The main conclusions are as follows:

1. A single-stranded hairpin conformation was observed for HP in its lowest charge state. However, PK was present in only a pseudoknot conformation in it lowest charge state, indicating that, for sequences where both a hairpin and pseudoknot conformation are possible, the pseudoknot conformation appears to be more favorable because of the extra WC pairing interactions.

2. As the charge states for the single-stranded HP and PK complexes became more negative, the WC pairs broke, and the strands elongated, eventually resulting in the complete loss of the hairpin and pseudoknot structures. This result brings forth the question of whether extended strands exist in solution or whether the increase in charge repulsion causes compact single-stranded complexes to open upon solvent evaporation.

3. HP did not form a double-stranded cruciform in the experiments, apparently because a single-stranded hairpin conformation is energetically favored over a cruciform with WC pairing mismatches for short self-complementary DNA strands (<23 bases). (There were too many mismatches for PK to form a self-complementary cruciform.)

4. A hairpin conformation was not possible for CF1 or CF2, as neither strand had complementary ends (CCGG versus CGCG). This allowed the $(CF1 \cdot CF2)^{11-}$ species to form and exist as a B-form helix in solution. However, it was observed as both A- and B-form helices under the solvent-free conditions of the experiments, with the mismatched region popping open to yield a cruciform-type structure.

Acknowledgment. The support of the National Science Foundation under Grant CHE-0503728 is gratefully acknowledged.

References and Notes

(1) Watson, J. D.; Crick, F. H. *Nature* **1953**, *171*, 1303.
(2) Singleton, C. K. *J. Biol. Chem.* **1983**, *258*, 7661.
(3) Sullivan, K. M.; Lilley, D. M. *J. Mol. Biol.* **1987**, *193*, 397.
(4) Glucksmann, M. A.; Markiewicz, P.; Malone, C.; Rothman-Deenes, L. B. *Cell* **1992**, *70*, 491.
(5) Larsen, A.; Weintraub, H. *Cell* **1982**, *29*, 609.
(6) Huertas, D.; Azorin, F. *Biochemistry* **1996**, *35*, 13125.
(7) Heller, M. J. *Annu. Rev. Biomed. Eng.* **2002**, *4*, 129.
(8) Gaylord, B. S.; Heeger, A. J.; Bazan, G. C. *Proc. Natl. Acad. Sci. U.S.A.* **2002**, *99*, 10954.
(9) Tyagi, S.; Kramer, F. R. *Nat. Biotechnol.* **1996**, *14*, 303.
(10) Fan, C.; Plaxco, K. W.; Heeger, A. J. *Proc. Natl. Acad. Sci. U.S.A.* **2003**, *100*, 9134.
(11) von Helden, G.; Hsu, M.-T.; Kemper, P. R.; Bowers, M. T. *J. Chem. Phys.* **1991**, *95*, 3835.
(12) Wyttenbach, T.; von Helden, G.; Bowers, M. T. *Int. J. Mass Spectrom. Ion Proc.* **1997**, *165/166*, 377.
(13) Wyttenbach, T.; Bowers, M. T. *Top. Curr. Chem.* **2003**, *225*, 207.
(14) Wyttenbach, T.; Kemper, P. R.; Bowers, M. T. *Int. J. Mass Spectrom.* **2001**, *212*, 13.
(15) Mason, E. A.; McDaniel, E. W. *Transport Properties of Ions in Gases*; Wiley, New York, NY, 1988.
(16) *HyperChem 7.0*; Hypercube Inc.: Gainesville, FL, 2002.
(17) Case, D. A.; Pearlman, D. A.; Caldwell, J. W.; Cheatham, T. E., III; Wang, J.; Ross, W. S.; Simmerling, C. L.; Darden, T. A.; Merz, K. M.; Stanton, R. V.; Cheng, A. L.; Vincent, J. J.; Crowley, M.; Tsui, V.; Gohlke, H.; Radmer, R. J.; Duan, Y.; Pitera, J.; Massova, I.; Seibel, G. L.; Singh, U. C.; Weiner, P. K.; Kollman, P. A. *AMBER 7*; University of California: San Francisco, 2002.
(18) Mesleh, M. F.; Hunter, J. M.; Shvartsburg, A. A.; Schwartz, G. C.; Jarrold, M. F. *J. Phys. Chem.* **1996**, *100*, 16082.
(19) Shvartsburg, A. A.; Jarrold, M. F. *Chem. Phys. Lett.* **1996**, *261*, 86.
(20) Lee, S.; Gotts, N. G.; von Helden, G.; Bowers, M. T. *Science* **1995**, *267*, 999.
(21) Wyttenbach, T.; von Helden, G.; Bowers, M. T. *J. Am. Chem. Soc.* **1996**, *118*, 8355.
(22) Wyttenbach, T.; Bushnell, J. E.; Bowers, M. T. *J. Am. Chem. Soc.* **1998**, *120*, 5098.
(23) Hoaglund, C. S.; Liu, Y.; Ellington, A. D.; Pagel, M.; Clemmer, D. E. *J. Am. Chem. Soc.* **1997**, *119*, 9051.
(24) Gidden, J.; Ferzoco, A.; Baker, E. S.; Bowers, M. T. *J. Am. Chem. Soc.* **2004**, *126*, 15132.
(25) Baker, E. S.; Bowers, M. T. *J. Am. Soc. Mass Spectrom.* **2007**, *18*, 1188.
(26) Gidden, J.; Baker, E. S.; Ferzoco, A.; Bowers, M. T. *Int. J. Mass Spectrom.* **2005**, *240*, 183.
(27) Veenstra, T. D. *Biochem. Biophys. Res. Commun.* **1999**, *257*, 1.
(28) Riazance, J. H.; Baase, W. A.; Johnson, W. C., Jr.; Hall, K.; Cruz, P.; Tinoco, I., Jr *Nucleic Acids Res.* **1985**, *13*, 4983.
(29) Segersnolten, G. M. J.; Sijtsema, N. M.; Otto, C. *Biochemistry* **1997**, *36*, 13241.
(30) Poehl, F. M.; Jovin, T. M. *J. Mol. Biol.* **1972**, *67*, 375.
(31) Trantirek, L.; Stefl, R.; Vorlickova, M.; Koca, J.; Sklenar, V.; Kypr, J. *J. Mol. Biol.* **2000**, *297*, 907.
(32) Franklin, R. E.; Gosling, R. G. *Acta Crystallogr.* **1953**, *6*, 673.

JP807529M